Bacterial immunogenic α-galactosylceramide identified in the murine large intestine: dependency on diet and inflammation[S]

Johanna von Gerichten,[*,†] Dominic Lamprecht,[*] Lukáš Opálka,[*,§] Daphnée Soulard,[**] Christian Marsching,[††] Robert Pilz,[*,†] Valentin Sencio,[**] Silke Herzer,[§§] Bruno Galy,[***] Viola Nordström,[§§] Carsten Hopf,[††] Hermann-Josef Gröne,[§§,†††] François Trottein,[**] and Roger Sandhoff[1,*]

Lipid Pathobiochemistry Group, Department of Cellular and Molecular Pathology,[*] Department of Cellular and Molecular Pathology,[§§] and Division of Virus-Associated Carcinogenesis,[***] German Cancer Research Center, Heidelberg, Germany; Faculty of Biosciences,[†] University of Heidelberg, Heidelberg, Germany; Skin Barrier Research Group,[§] Department of Organic and Bioorganic Chemistry, Faculty of Pharmacy in Hradec Králové, Charles University, Hradec Králové, Czech Republic; Centre d'Infection et d'Immunité de Lille,[**] Inserm U1019, CNRS UMR 8204, University of Lille, CHU Lille, Institut Pasteur de Lille, Lille, France; Center for Mass Spectrometry and Optical Spectroscopy (CeMOS),[††] Mannheim University of Applied Sciences, Mannheim, Germany; and Institute of Pharmacology,[†††] University of Marburg, Marburg, Germany

Abstract The glycosphingolipid, α-galactosylceramide (αGalCer), when presented by CD1d on antigen-presenting cells, efficiently activates invariant natural killer T (*i*NKT) cells. Thereby, it modulates immune responses against tumors, microbial and viral infections, and autoimmune diseases. Recently, the production of αGalCer by *Bacteroidetes* from the human gut microbiome was elucidated. Using hydrophilic interaction chromatography coupled to MS^2, we screened murine intestinal tracts to identify and quantify αGalCers, and we investigated the αGalCer response to different dietary and physiologic conditions. In both the cecum and the colon of mice, we found 1–15 pmol of αGalCer per milligram of protein; in contrast, mice lacking microbiota (germ-free mice) and fed identical diet did not harbor αGalCer. The identified αGalCer contained a β(*R*)-hydroxylated hexadecanoyl chain *N*-linked to C18-sphinganine, which differed from what has been reported with *Bacteroides fragilis*. Unlike β-anomeric structures, but similar to αGalCers from *B. fragilis*, the synthetic form of the murine αGalCer induced *i*NKT cell activation in vitro. Last, we observed a decrease in αGalCer production in mice exposed to conditions that alter the composition of the gut microbiota, including Western type diet, colitis, and influenza A virus infection. Collectively, this study suggests that αGalCer is produced by commensals in the mouse intestine and reveals that stressful conditions causing dysbiosis alter its synthesis. The consequences of this altered production on *i*NKT cell-mediated local and systemic immune responses are worthy of future studies.—von Gerichten, J., D. Lamprecht, L. Opálka, D. Soulard, C. Marsching, R. Pilz, V. Sencio, S. Herzer, B. Galy, V. Nordström, C. Hopf, H-J. Gröne, F. Trottein, and R. Sandhoff. **Bacterial immunogenic α-galactosylceramide identified in the murine large intestine: dependency on diet and inflammation. *J. Lipid Res*. 2019.** 60: **1892–1904.**

Supplementary key words glycolipids • sphingolipids • mass spectrometry • immunology • bacteria • invariant natural killer T cells • Western diet • experimental colitis • influenza A virus • cluster of differentiation 1d

Besides recognition of classical major histocompatibility complex class I or II molecules presenting oligopeptides by T lymphocytes, a wide variety of nonclassical nearly monomorphic major histocompatibility complex molecules, including CD1, may be recognized by αβ and γδ T cells as

This work was supported in part by the Institut National de la Santé et de la Recherche Médicale, the Centre National de la Recherche Scientifique, the University of Lille, the Pasteur Institute of Lille, and l'Agence Nationale de la Recherche (AAP générique 2017, ANR-17-CE15-0020-01, ACROBAT) (F.T.). S.H. received funding from Deutsche Forschungsgemeinschaft Grant HE 7978/1-1.

Manuscript received 2 July 2019 and in revised form 22 August 2019.

Published, JLR Papers in Press, September 4, 2019
DOI https://doi.org/10.1194/jlr.RA119000236

Abbreviations: APC, antigen-presenting cell; CID, collision-induced dissociation; DC, dendritic cells; DSS, dextran sodium sulfate; FT-ICR, Fourier transformation-ion cyclotron resonance; GalCer, galactosylceramide; αGalCer, α-galactosylceramide; $\alpha GalCer_{Bf}$, α-galactosylceramide (d(17/18/19):0/βh17:0) from *Bacteroides fragilis*, which incorporates three isobranched sphingoid bases with a total of 17, 18, and 19 carbon atoms; $\alpha GalCer_{MLI}$, α-galactosylceramide(d18:0/βh16:0) from murine large intestine; GlcCer, glucosylceramide; HexCer, hexosylceramide; HILIC, hydrophilic interaction chromatography; IAV, influenza A virus; IL-2, interleukin-2; *i*NKT, invariant natural killer T; KRN7000, α-galactosylceramide(d18:0/t26:0); LCB, long chain base (of ceramide); McL, McLafferty (fragment); MLI, mouse large intestine; MRM, multiple reaction monitoring; NKT, natural killer T; RP18, reversed phase 18 C-atoms; TCR, T cell receptor; WTD, Western type diet.

[1]To whom correspondence should be addressed.
e-mail: r.sandhoff@dkfz.de

[S] The online version of this article (available at http://www.jlr.org) contains a supplement.

well as natural killer T (NKT) cells. These "unconventional" T cells recognize lipids, metabolites, and modified peptides (1). The glycosphingolipid, α-galactosylceramide (αGalCer), presented by CD1d of antigen-presenting cells (APCs) is one of the most potent stimulators of invariant NKT (*i*NKT) cells (2, 3). The interaction of the presented lipid-CD1d complex with the T cell receptor (TCR) of *i*NKT cells can activate these cells and trigger the release of a variety of cytokines and chemokines modulating immune responses (4, 5).

Originally, αGalCer was found in the marine sponge, *Agelas mauritianus*, in 1993 (6), and still, to date, very little is known about natural contact of mammalian organisms with this sphingolipid either through microbial sources or by endogenous production. Later, *Bacteroides fragilis*, a commensal of the human gut, was demonstrated to produce αGalCer ($\alpha GalCer_{Bf}$) (7). Based on this work, two more strains of the human gut microbiome, *Bacteroides vulgatus* and *Prevotella copri*, were demonstrated to produce αGalCer (8). Recent work has shown that early exposure to $\alpha GalCer_{Bf}$ reduces *i*NKT cell number in the mouse colon, thereby protecting against colitis (9). Hence, there is a need to identify structure-specific sphingolipids in the gut microbiome to elaborate the role of bacterial sphingolipids in the host-immune response.

As mentioned, the immunogenic αGalCers belong to the class of sphingolipids that all contain a long chain base (LCB) 2-amino alcohol. In most cases, the LCB is amide linked with a fatty acyl chain to form ceramides, which often are modified at C1-position to carry a head group, such as various glycans, phosphorylcholine, phosphate, or acyl chains. The LCB as well as the fatty acyl residue can vary in their chain lengths, methylation, and degree of saturation and hydroxylation, and thereby create a huge variety of ceramide backbones, which contribute additionally to the variation and complexity of the sphingolipid class (10, 11). Sphingolipids are known to play important roles in proliferation, apoptosis, differentiation, and migration of eukaryotic cells (12–16). In contrast, only a few bacteria are known to produce sphingolipids (17–19). Among them is *B. fragilis*, which has recently been described to produce αGalCer with a C17, C18, or C19 iso-branched sphinganine LCB and a β-hydroxylated C17 iso-branched fatty acyl residue (7, 9). These structures were also present in *Bacteroides vulgatus* and *P. copri* (8). Human pathology with diseases such as diarrhea, inflammatory bowel disease, and cancer were connected to the abundance of *B. fragilis* in the human gut (7, 20–22). In the mouse system, there is evidence that the gut microbiota can produce *i*NKT cell agonists (23, 24). However, the nature of these agonists has not yet been clearly defined.

MS has become the most accurate tool to measure lipids. Although, structural stereoisomers often cannot be separated by MS alone, the combination of MS with LC can be suited to distinguish them. Our group recently published a method to successfully separate α- and β-anomeric isomers of glucosylceramide (GlcCer) and GalCer (8). This method has now enabled us to screen mouse intestinal tissue and content for hexosylceramide (HexCer) structures with an α-glycosidic linkage produced by bacteria. In the current report, we describe the identification of an αGalCer structure originating from the gut microbiome. This αGalCer was absent in microbiota-deficient mice. Because the low concentration of this compound did not allow us to obtain sufficient purified material for structural NMR analysis, we chemically synthesized the assumed structure in an α- and β-anomeric form. This allowed us to reveal the differential behavior of these compounds in hydrophilic interaction chromatography (HILIC) and MS collision-induced dissociation (CID) similar to previously described differential CID-fragmentation patterns (7, 25–28). By that, we subsequently confirmed the mouse intestinal tract-derived compound as αGalCer(d18:0/βh16:0)[2] containing C18-sphinganine and a β-hydroxylated palmitic acid. Furthermore, this α-anomeric compound turned out to stimulate *i*NKT cells in a similar manner as the αGalCers from *B. fragilis*. We further show that the production of αGalCer(d18:0/βh16:0) largely fluctuates according to the diet, local inflammatory conditions, and infection. These data imply that alteration of the microbiome composition impacts strongly on αGalCer production.

MATERIALS AND METHODS

Sphingolipids and reagents

αGalCer(d18:1/16:0), βGalCer(d18:1/16:0), αGalCer(d18:0/16:0), βGalCer(d18:0/16:0), βGalCer(d18:1/α(*R*)h18:0), βGalCer(d18:1/α(*S*)h18:0), α/βGalCer(d18:1/24:1), α/βGlcCer(d18:1/24:1), βGlcCer(d18:1/16:0), C18-α-galactosylsphingosine, and C18-α-glucosylsphingosine were purchased from Avanti Polar Lipids. Kerasin (nonhydroxylated acyl chain containing βGalCers from bovine brain) and phrenosin (α-hydroxylated acyl chain containing βGalCers from bovine brain) were from Matreya. C18-β-galactosylsphingosine (psychosine) was purchased from Abcam. Racemic β-hydroxypalmitic acid, 1-hydroxybenzotriazole hydrate, 4-dimethylaminopyridin, anthrone, and *N*-(3-dimethylaminopropyl)-*N*′-ethylcarbodiimide were provided by Sigma-Aldrich. A mix of βGlcCer(d18:1/14:0, 19:0, 25:0) and βGalCer(d18:1/31:0) was used as internal standard. These internal standard compounds had previously been chemically synthesized from the corresponding commercially available βGlcSph(d18:1) or βGalSph(d18:1) and dicyclohexylcarbodiimide/*N*-hydroxysuccinimide-activated commercially available free fatty acids, and were quantified using the anthrone test and thin-layer chromatography (29) as described in detail earlier (30).

Solvents and additives

Anhydrous (dry) tetrahydrofuran was purchased from Sigma-Aldrich. Chloroform, methanol, isopropanol, water, all LC-MS Chromasolv®-grade, and 2-butanol (≥99.5%) for GC were from Honeywell Specialty Chemicals Seelze GmbH; propionitrile for synthesis was from Merck Darmstadt; formic acid (99–100%) was from VWR International; ammonium acetate and ammonium formate (≥99%) for MS-analytics were from Sigma-Aldrich.

[2] Ceramide anchor description of hexosylceramides: In GalCer(d18:0/βh16:0), the first code (d18:0) refers to the sphingoid base (LCB), in this case with two hydroxyl groups (d), 18 carbon atoms, and no double bonds (0), and the second code (βh16:0) refers to the amide linked acyl chain (fatty acyl) containing, in this case, one hydroxyl group (h) in β-position, 16 carbon atoms and no double bond (0).

Mice

Tissue was isolated from euthanized C57BL/6N, C57BL/6J, and NMRI mice. Mice were obtained from the animal facilities of the German Cancer Research Center, the EMBL in Heidelberg, and the Pasteur Institute in Lille, as well as Charles River, Sulzfeld. Except for germ-free mice (NMRI-held in the animal facility of the German Cancer Research Center), all mice were kept under specific pathogen-free conditions. All animal procedures were approved by the respective governmental institutions and performed in accordance with federal laws. Duodenum was cut out 2 cm following stomach, and jejunum was taken from the middle of the small intestine, both with a length of about 1 cm. The dead-end part (1 cm) of caeca was cut out and, with a distance of 2 cm from cecum, colon tissue samples with the length of 1 cm were cut and immediately stored at −80°C. Feces were obtained from the rectum. *CD1d*$^{-/-}$ mice, backcrossed at least 10 times in C57BL/6, were a gift from Dr. L. Van Kaer (Vanderbilt University, Nashville, TN).

Bacteria

According to previous publication (31), *B. fragilis* (DSM-2151) was grown anaerobically on Columbia agar plates with 5% sheep blood for 48 h. One culture plate was harvested and transferred in a tube containing 200 μl of methanol.

Chemical synthesis of hexosylceramides

For the synthesis and quantification of αGlcCer, αGalCer, and βGalCer standards carrying a β-hydroxylated fatty acid, see the supplemental Methods.

Lipid extraction

For the enrichment of HexCers containing GalCer(d18:0;h16:0) from a larger amount of mouse caeca and lipid extraction from small amounts of mouse tissue as well as lipid extraction from bacteria, see the supplemental Methods.

HILIC- and reversed-phase LC-MS^2 analysis of GalCer

Aliquots corresponding to 10 mg of mammalian tissue dry weight or rather 2 mg of dried bacteria were mixed with internal lipid standards for analysis by LC-MS^2 using an Acquity I-class UPLC and a Xevo TQ-S "triple quadrupole" instrument, both from Waters. Using a CSH C18 column (2.1 × 100 mm, 1.7 μm; Waters), lipids were measured in reversed-phase-LC mode with a gradient between 57% solvent A (50% methanol) and 99% solvent B (1% methanol, 99% isopropanol), both containing either 10 mM of ammonium acetate or 0.1% formic acid and 10 mM of ammonium formate as additives (supplemental Table S1). In HILIC mode, lipids were separated on a CORTECS HILIC column (2.1 × 150 mm, 1.6 μm; Waters) using a gradient between 100% solvent A (97% propionitrile, 2% 2-butanol, and 1% water) and 100% solvent B (97% methanol, 2% 2-butanol, 1% of an aqueous 10 mM ammonium formate solution), both containing 0.1% formic acid as an additive (supplemental Table S2). From the extracted samples, 0.05–0.1% corresponding to 5–10 μl was injected for measurement. Lipids analyzed were detected by multiple reaction monitoring (MRM) (supplemental Tables S3, S4). To increase the sensitivity of the mass spectrometric detection in HILIC mode, a solution of 120 mM of ammonium formate in methanol was blended uniformly with the 0.35 ml/min eluate from the HILIC column for ESI at a flow rate of 10 μl/min. GlcCer(d18:1;14:0), GlcCer(d18:1;19:0), GlcCer(d18:1;25:0), and GalCer(d18:1;31:0) were used as internal standards to quantify α- and β-anomers of GlcCer and GalCer, taking methodological response differences between HexCers with sphingosine and sphinganine as evaluated with external standards into account. Student's *t*-test was conducted with GraphPad Prism (GraphPad Software, San Diego, CA) and $P \leqslant 0.05$ was considered to be statistically significant. Data were presented as the mean ± standard deviation.

High resolution FT-ICR-MS^2 analysis of αGalCer$_{MLI}$

Fourier transformation-ion cyclotron resonance (FT-ICR)-MS and -MS^2 were performed on a solariX 7T XR magnetic resonance mass spectrometer (Bruker Daltonics) equipped with a dual ESI/MALDI ion source. Spectra were acquired in ESI positive ion mode with a size of 4M data points and active absorption mode; transfer time-of-flight was 0.700 ms, and the Q1 mass was set on the mass of interest to achieve highest sensitivity. Calibration was performed on clusters of sodium formate followed by internal lock mass calibration for MS^2 on the precursor ion of interest. For each spectrum in MS mode, 20 scans with an accumulation time of 0.01 s were added, and in MS^2 mode, 200–800 scans with an accumulation time of 1.1 s were added. CID fragmentation was performed with a collision energy of 25 V after isolating the respective precursor with a width of ±0.1 Da.

Activation of *i*NKT cells with lipids

To generate dendritic cells (DCs), bone marrow precursors from wild-type mice were cultured in complete IMDM medium supplemented with 10% FCS and 1% of a supernatant from a granulocyte-macrophage colony-stimulating factor-expressing cell line for 14 days. To investigate *i*NKT cell reactivity, 1×10^5 DCs (>90% purity) were cultured with 1×10^5 mouse *i*NKT hybridoma DN32.D3 (a gift from A. Bendelac, Chicago, IL) in the presence of purified glycolipids or vehicle in complete RPMI medium supplemented with 5% FCS for 24 h. Glycolipids were added from a stock solution of 0.1 mg/ml in PBS containing 0.05% Tween 20. Coculture supernatants were collected, and cytokine [interleukin-2 (IL-2)] production was measured by ELISA (R&D Systems, Minneapolis, MN). To assess activation of primary *i*NKT cells, splenocytes (10^6 cells/well, 96-well plate) were exposed to purified glycolipids or vehicle alone for 48 h. Supernatants were collected, and IFN-γ concentration was measured by ELISA (R&D Systems).

Treatment of mice with Western type diet

Male C57BL/6 mice (age 23–36 weeks) were housed in a controlled environment with free access to food and water. The mice were fed a Western type diet (WTD) (EF TD88137, ssniff special diets GmbH, Germany, containing 21.1 % fat, 14.4% polysaccharides, 34.3% sugar, and 0.21 % cholesterol) or a standard rodent diet (control; Altromin, Lage, Germany; #1310, containing 5.1% fat, 35% polysaccharides, and 5% sugar) for 7 days and euthanized afterwards by cervical dislocation. Tissue was removed quickly, weighed, and stored at −80°C until sample preparation.

Induction of colitis in mice

Nine- to 11-week-old C57BL/6 male mice were given 2% dextran sodium sulfate (DSS) (colitis grade, molecular weight 36,000–50,000; MP Biomedicals GmbH, Eschwege, Germany) in drinking water and euthanized, respectively, after 2 or 4 days of treatment. Induction of colitis was verified by performing an occult blood test (Hemoccult; Beckman Coulter GmbH, Krefeld, Germany) after 4 days of exposure to DSS.

Lung infection of mice with influenza A virus

Eight-week-old male C57BL/6 mice were purchased from Janvier (Le Genest-St-Isle, France). For infection with influenza A virus (IAV), mice were maintained in a biosafety level 2 facility in the Animal Resource Center at the Pasteur Institute, Lille. Mice

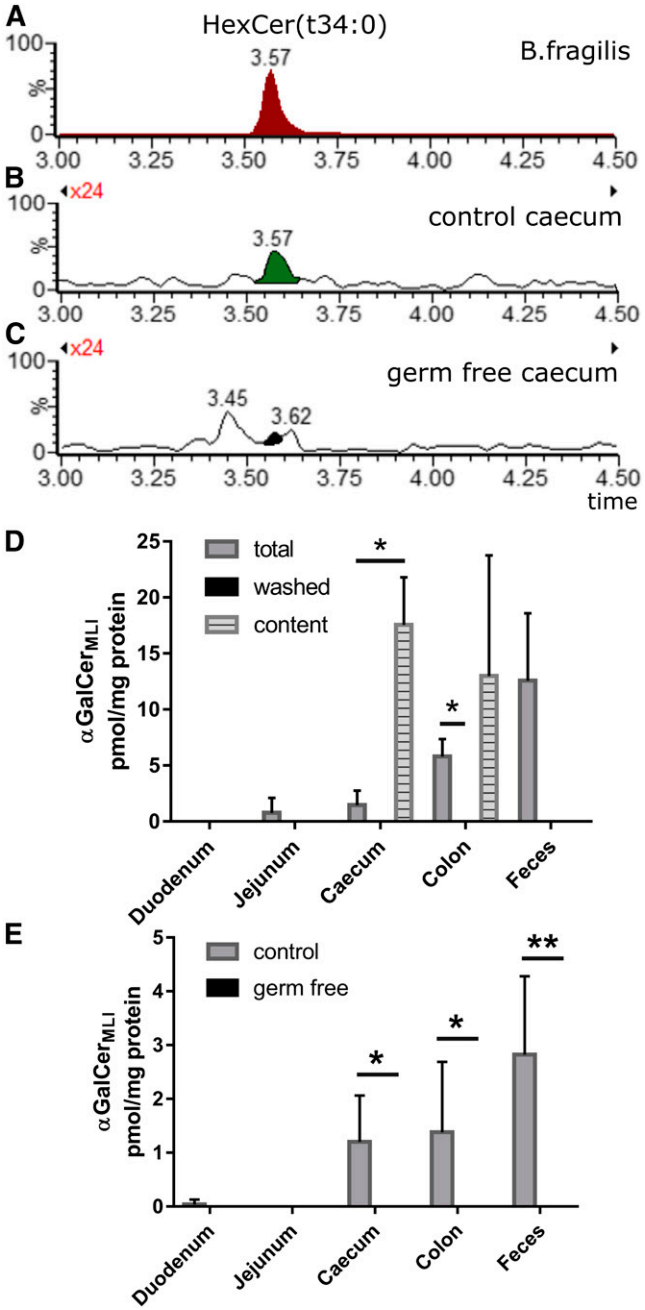

Fig. 1. HILIC-MS^2 reveals a potential microbial αGalCer(t34:0) obtained from murine large intestine samples. A–D: HILIC-MS^2. A: Extracted ion chromatogram (EIC): Detection of αGalCer(t34:0) from purified sphingolipids of *B. fragilis* (termed αGalCer$_{Bf}$) with SRM transition *m/z* 740.5 ($[M + H]^+$) to *m/z* 270.3 ($[Sa(d17:0) + H - H_2O]^+$), i.e., containing d17:0-sphingoid base and h17:0-acyl chain. B, C: EIC: Detection of GalCer(d18:0/h16:0) with SRM transition *m/z* 740.5 ($[M + H]^+$) to *m/z* 284.3 ($[Sa(d18:0) + H - H_2O]^+$) from total cecum (including luminal content) lipid extracts of mice with commensals (control) (B) and mice not harboring commensals (germ-free) (C). This GalCer(d18:0/h16:0) with identical retention time to αGalCer$_{Bf}$ is decribed further on as αGalCer$_{MLI}$. D: Quantities of αGalCer$_{MLI}$ at retention time = 3.57 min in extracts of tissues from 14-week-old male C57BL/6N mice including luminal content (total), tissues without luminal content (washed), and corresponding released luminal contents (n = 3). E: RP18-LC-MS^2. Quantification of αGalCer$_{MLI}$ from 14- to18-week-old male and female NMRI mice using specific transitions for αHexCer as outlined in the Materials and Methods. Extracts of tissues included luminal content, both from commensal containing (control) and germ-free mice. Note that αGalCer$_{MLI}$ is enriched in intestinal luminal contents, but disappears in tissues of germ-free mice (control, n = 6; germ free, n = 3). *$P < 0.05$; **$P < 0.01$; ***$P < 0.001$.

were anesthetized and administered intranasally with 50 μl of PBS containing [or not (mock)] 30 plaque-forming units of the high-pathogenicity murine-adapted H3N2 IAV strain, Scotland/20/74, as reported previously (32). Mock-treated and IAV-infected mice were euthanized at day 7 postinfection.

RESULTS

Screening of lipid extracts from mouse intestine by HILIC-MS^2 revealed the presence of a potential microbial αGalCer isomer

We previously reported a HILIC-MS^2 method to successfully separate GlcCers and GalCers as well as α- and β-HexCer isomers, showing the detection of α-glycosidically linked GalCers (αGalCers) from bacteria (8). Based on published structures for bacterial αGalCer, we screened mouse intestinal tissue for these and similar αGalCer structures by MRM in positive ESI mode. The mass spectrometric transitions used a sphingoid base-based fragment, indicating by that the size or chain length of the incorporated sphingoid base. In total cecum of C57BL/6N mice, we initially found a HexCer peak that migrated at the same retention time as αGalCer(d17:0;βh17:0), one of the main αGalCers from *B. fragilis* (αGalCer$_{Bf}$). The caecal HexCer had the same chemical formula, but appeared with the MRM transition for a C18-sphinganine (d18:0)-containing compound. Therefore, the attached hydroxylated fatty acid could only contain 16 carbons, HexCer(d18:0;h16:0). This peak, however, was absent in the cecum of germ-free NMRI mice (**Fig. 1A**–C). When separating cecum tissue from its luminal content, this peak disappeared from the washed caecum and increased in the content of caecum (Fig. 1D). Further investigations showed that this peak was basically absent in the duodenum and jejunum, but present in the content of cecum and colon as well as in feces (Fig. 1D). As it is present basically in the mouse large intestine (MLI), we name the structure here αGalCer$_{MLI}$. When comparing corresponding tissue of germ-free NMRI mice with control NMRI mice, this compound was only found in control mice but not in germ-free mice (Fig. 1E). These data implicate a bacterial origin of the αGalCer$_{MLI}$ peak, which is supported by its enrichment in the corresponding tissue contents and depletion in intestinal tissue lacking content (Fig. 1D).

The HILIC-MS^2 results lead us to the hypothesis that, as attributed to αGalCer$_{Bf}$, this peak from the mouse large intestine would contain an α-glycosidically linked galactosyl residue and a β-hydroxylated acyl chain, the latter *N*-linked to a dihydrosphingosine base, but, in contrast to αGalCer$_{Bf}$, with an even number of C-atoms in both the LCB and the fatty acyl chain.

Analyzing sodium adducts of GalCers by LC-MS^2 displays structural information on anomeric linkage of the sugar moiety and β-hydroxylation of the acyl chain

We next turned to prove the anomeric linkage of the sugar moiety and the position of the hydroxyl group in the acyl chain. Due to the low concentration of $\alpha GalCer_{MLI}$ in cecum tissue with no more than 80 ng per single mouse cecum, we excluded NMR studies and focused on LC-MS^2 analysis relying on characteristic CID-generated product ion patterns for structure elucidation: First, Brennan et al. (25) previously demonstrated differences in the fragmentation spectra between α- and βGalCer-containing nonhydroxylated acyl chains when selecting the sodiated molecular ions for CID. Basically, the ratio of the product ions $[GalCer + Na - hexose]^+$ (fragment c in **Fig. 2A**) over $[GalCer + Na - (hexose - H_2O)]^+$ (fragment b in Fig. 2A) decreased significantly in the α-anomer, which we also saw analyzing commercially available GalCer(d18:1/16:0) and GalCer(d18:0/16:0) standards (Fig. 2B–E). Second, Brown et al. (7) reported a specific product ion to appear from the deprotonated αGalCer ion (−ESI) containing a β-hydroxylated fatty acyl chain. This ion corresponds to a similar product ion reported in the CID-spectra of a deprotonated ceramide ion from mouse skin, which also contains a β-hydroxylated fatty acyl chain and likely is derived by McLafferty (McL) fragmentation (33). This type of β-cleavage apparently depends on β-hydroxylation of the acyl chain.

To evaluate the fragmentation behavior of GalCer with β-hydroxylated acyl chains, we synthesized and quantified GalCer standards with a β-hydroxylated acyl chain [α-, βGalCer(d18:1/βh16:0); α-, βGalCer(d18:0/βh16:0)] as described in Materials and Methods. Due to the incorporation of racemic β(*R/S*)-hydroxylated palmitic acid into the corresponding chiral galactosylsphingosines, each synthesis yielded a mixture of two diastereomeric compounds, which migrated as double bands on thin-layer chromatography as well as double peaks on reversed phase 18 C-atoms (RP18)-LC (supplemental Fig. S1). On RP18-LC, β-hydroxylated GalCers eluted earlier than α-hydroxylated GalCers, which again eluted in front of the corresponding nonhydroxylated compounds (supplemental Fig. S1). CID-product ion spectra derived from the first peak of the double peak did not differ from the corresponding second peak for all four compound mixtures (supplemental Fig. S2). Comparison of CID-product ion spectra of α- and βGalCers containing a C18-LCB and a C16-acyl chain revealed a specific McL fragment [*m/z* 526 for α/βGalCer(d18:1/βh16:0) and *m/z* 528 for α/βGalCer(d18:0/ βh16:0)] to appear in the spectra of compounds with a β-hydroxylated acyl chain (Fig. 2F–I), but not in spectra of those compounds containing nonhydroxylated or α-hydroxylated acyl chains [*m/z* 526 and 528 not observed for α/βGalCer(d18:1/16:0) and α/βGalCer(d18:0/16:0), Fig. 2B–E; *m/z* 542 or 524 not observed for βGalCer(d18:1/α(*R/S*)18:0), Fig. 2J, K]. The McL fragment in GalCers with a β-hydroxylated acyl chain was accompanied by another peak due to the subsequent loss of the sugar moiety from the McL fragment (supplemental Fig. S2). Spectra of compounds with an α-hydroxylated acyl chain contained a characteristic low intense fragment e (*m/z* 512) not present in spectra of GalCer with nonhydroxylated or β-hydroxylated acyl chains (Fig. 2J, K). The other fragments (a, b, c, and d), which are due to water, sugar, or acyl chain loss, appeared in all compounds as well as *m/z* 203 representing the release of sodiated galactose (supplemental Fig. S2). To address differences in the product ion spectra arising from the anomeric linkage of the galactosyl residue, we compared the CID spectra of corresponding pairs of αGalCer and βGalCer standards with identical ceramide anchor. The fragmentation pattern detected was qualitatively the same for corresponding pairs of α- and β-glycosidically linked GalCers. Differences were observed in the relative abundance of these fragments. As reported previously (25), the α- and β-anomers of GalCer with nonhydroxy acyl chains differed in the ratio of fragment b over fragment c in favor of b in spectra of the αGalCers. In spectra of GalCers containing β-hydroxylated acyl chains, fragment c almost disappeared. However, we found a quantitative difference in the abundance of the McL fragment over fragment b in favor of the McL fragment in β-anomeric compounds (Fig. 2F–I). These results encouraged us to adopt the b/McL fragment ratio as a marker for the anomeric structure of GalCers with β-hydroxylated acyl chains. Therefore, we determined the optimal collision energies for the corresponding MS^2 transitions (supplemental Fig. S3). With optimized parameters, all standards were then subjected to RP18-LC-MS^2 and monitored by MRM transitions of the molecular sodium adducts to fragments a, b, c, d, e, and McL. Standards with β-hydroxylated acyl chains again revealed double peaks, as they represented diastereomeric mixtures as stated above (supplemental Fig. S4). Relative quantification of the transitions revealed a highly significant (more than 15-fold) difference in the b/McL ratio between corresponding α- and β-anomeric compounds, independent of the *R/S*-orientation of the β-hydroxy group (supplemental Fig. S5).

$\alpha GalCer_{MLI}$ enriched from mouse cecum is indistinguishable from the synthetic αGalCer(d18:0;βh16:0) by RP18-LC-MS^2

Next, we enriched GalCers from a pool of mouse caeca to increase signal intensities for further analysis, as described in the Materials and Methods. By RP18-LC-MS^2, the enriched sample contained two peaks of HexCer(d18:0;h16.0). The first and main peak ($\alpha GalCer_{MLI}$) eluted identically to the second peak of the synthetic α- and βGalCer(d18:0:βh16:0) standards but 0.15 min later than αGalCer(d17:0;βh17:0) from *B. fragilis* (**Fig. 3A**). Monitoring the above identified fragments in relative quantity by MRM, the $\alpha GalCer_{MLI}$ peak was again not distinguishable from αGalCer(d18:0:βh16:0), but the b/McL ratio clearly differed from the corresponding β-anomer (Fig. 3B). Additionally, the fragmentation patterns of all three αGalCers detected in *B. fragilis* ($\alpha GalCer_{Bf}$) were identical to the major peak from the enriched cecum sample, except for differences in the chain length of the sphingoid base and acyl chain. The fragmentation pattern of the second minor HexCer(d18:0:h16:0)

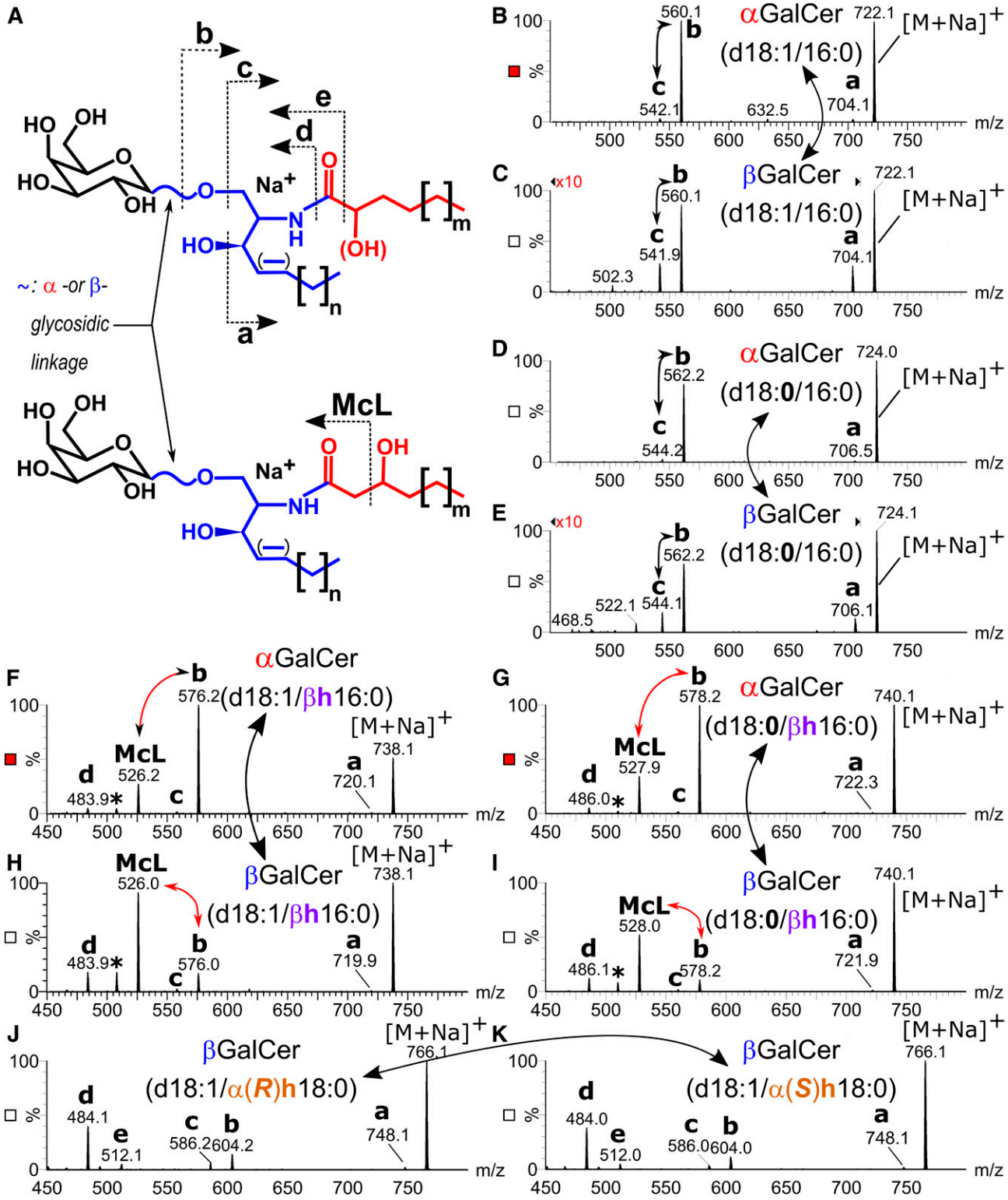

Fig. 2. Product ion spectra of sodium adducts of synthetic GalCers. A: Structure of GalCers with nonhydroxylated and α-hydroxylated acyl chains (upper structure), and with β-hydroxylated acyl chains (lower structure) including fragmentation pattern to fragments a, b, c, McL, d, and e. B–K: Production ion spectra induced by CID (45 V) of αGalCer(d18:1/16:0) (B), βGalCer(d18:1/16:0) (C), αGalCer(d18:0/16:0) (D), βGalCer(d18:0/16:0) (E), αGalCer(d18:1/βh16:0) (F), αGalCer(d18:0/βh16:0) (G), βGalCer(d18:1/βh16:0) (H), βGalCer(d18:0/βh16:0) (I), βGalCer(d18:1/α(*R*)h18:0) (J), and βGalCer(d18:1/α(*S*)h18:0) (K). Note the difference in the b/c-ratio between α- and βGalCers with nonhydroxylated acyl chains (B–E), the unique McL fragment of GalCers with β-hydroxylated acyl chains and the difference in the b/McL-ratio between corresponding α- and βGalCers (F–I) as well as the unique fragment e from GalCers with α-hydroxylated acyl chains (J, K).

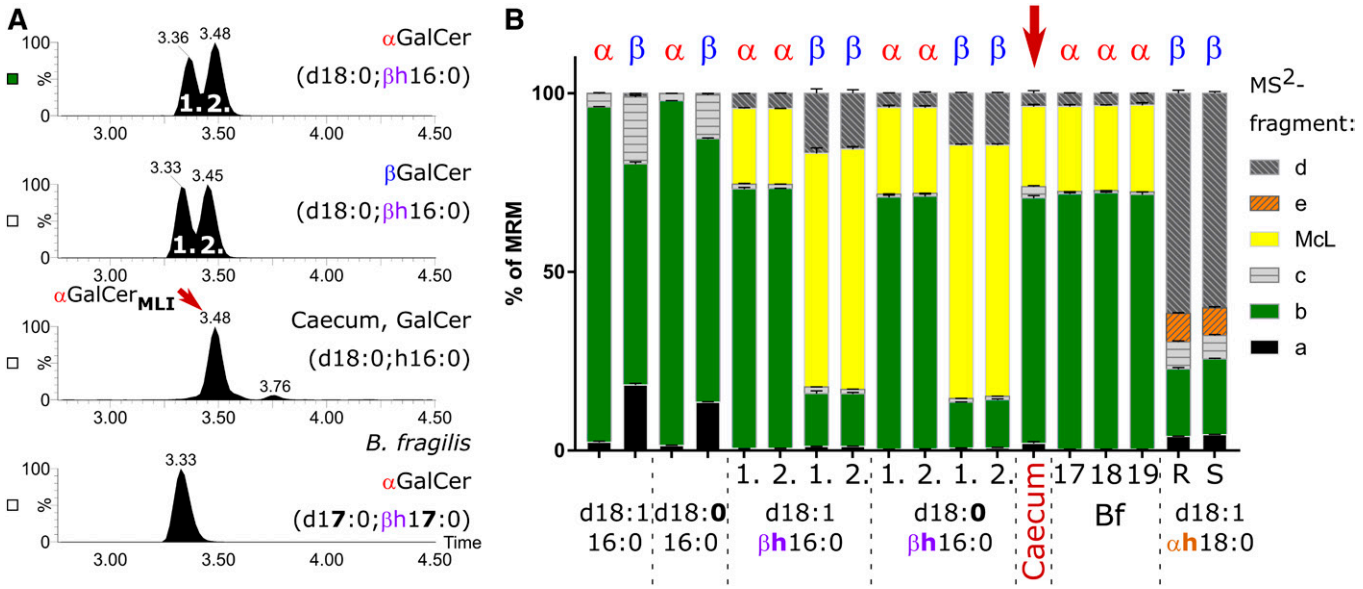

Fig. 3. Comparison of GalCer(d18:0;h16:0) from mouse cecum with synthetic GalCer standards and αGalCer from *B. fragilis* by MRM on RP18-LC. A: Total ion chromatograms resulting from MRM transition of the sodiated compounds to fragments a, b, c, McL, d, and e (see Fig. 2A, supplemental Table S5). The RP18-LC gradient contained 10 mM of ammonium acetate as additive. B: Relative abundance of the six monitored transitions for synthetic GalCer with a C18-base and a nonhydroxylated or β-hydroxylated C16:0-acyl chain, GalCer with a C18-base, and an α-hydroxylated C18:0 acyl chain, $\alpha GalCer_{MLI}$, enriched from mouse cecum as well as $\alpha GalCer_{Bf}$ with a C17- (17), C18- (18), or C19-base (19) from *B. fragilis* (Bf), each containing a β*R*-hydroxylated C17:0-acyl chain. Synthetic GalCers with a β-hydroxylated acyl chain represent each a diastereomeric mixture containing βR- and βS-hydroxylated C16:0 acyl chains. These diastereomeric mixtures elute as double peaks (see A), which are annotated in B with (1.) and (2.) for the first and the second peak. Note that an $\alpha GalCer_{MLI}$ from mouse cecum [main peak (A)] migrates with the second peak of synthetic αGalCer(d18:0/βh16:0) at 3.48 min. Furthermore, this $\alpha GalCer_{MLI}$ peak does not differ by fragmentation pattern from synthetic αGalCer(d18:0/βh16:0) nor from any αGalCer of *B. fragilis*. However, it significantly differs from that of βGalCer(d18:0/βh16:0). The $\alpha GalCer_{MLI}$ from cecum eluted 0.15 min later than αGalCer(d17:0/βh17:0) from *B. fragilis*, likely due to the iso-branching of the sphingoid base and acyl chain in the latter. The minor HexCer(d18:0/h16:0) peak of the cecum sample (here at 3.76 min) migrates with βGlcCer(d18:0/αh16:0) generated by hydration from mouse small intestine GlcCer(d18:1/αh16:0) (supplemental Fig. S6) (n = 3).

peak (retention time = 3.76 min) from the enriched cecum sample did not reveal a McL fragment, but revealed at a low intensity the fragment e, which had been observed in the standards containing α-hydroxylated acyl chains (Fig. 3B). These results confirm that the major HexCer(d18:0,h16:0) of mouse caeca, i.e., $\alpha GalCer_{MLI}$, is a αGalCer(d18:0;βh16:0) containing a β-hydroxylated fatty acyl and an α-glycosidic sugar linkage.

HILIC-MS^2 adds further evidence for the presence of αGalCer(d18:0;βh16:0) in mouse caeca

In our previous publication (8), we could show that not only GalCer can be separated from GlcCer with HILIC-MS^2, but also αGalCer from βGalCer. The method had been set up with HexCer standards containing nonhydroxylated acyl chains. Therefore, we compared the retention behavior of a β-hydroxylated acyl chain containing α/βGalCer standards with $\alpha GalCer_{MLI}$ from mouse cecum and with $\alpha GalCer_{Bf}$ by HILIC-MS^2. As by RP18-LC, every GalCer standard with a β-hydroxylated acyl chain revealed a double peak by HILIC-MS^2 due to the racemic presence of either the β*R*- or the β*S*-hydroxylated acyl chain. However, in contrast to GalCers with nonhydroxylated acyl chains, the double peaks of α- and-βGalCer with β-hydroxylated acyl chains eluted very similarly, with a minimal but significant difference of 0.03 min. Therefore, an equal mixture of the α- and -βGalCer standards, both containing a β-hydroxylated acyl chain, revealed no baseline separation, but yielded two broad peaks, each with a shoulder (**Fig. 4A–**C). When $\alpha GalCer_{MLI}$ from cecum was spiked with synthetic βGalCer(d18:0/βh16:0), the second of the double peaks broadened roughly by 50% (FWHH: first, 0.036 ± 0.003 min; second, 0.053 ± 0.009 min) and revealed a shoulder (Fig. 4F). Clearly $\alpha GalCer_{MLI}$ differed in structure from the corresponding βGalCer. Next, we spiked synthetic αGalCer(d18:0/βh16:0) into the enriched $\alpha GalCer_{MLI}$ from cecum. This time, the second of the standard double peaks remained a sharp peak (FWHH: first, 0.035 ± 0.002 min; second, 0.034 ± 0.001 min) without a shoulder, but, as expected, increased in intensity compared with the first peak (Fig. 4G, supplemental Fig. S7). These data further confirm the α-anomeric linkage of galactose in $\alpha GalCer_{MLI}$ from mouse cecum. In addition, $\alpha GalCer_{Bf}$(d17:0;βh17:0) migrated identically to this $\alpha GalCer_{MLI}$ (Fig. 4D, E), which implies a β*R*-configuration for the hydroxyl group in the acyl chain.

Because α- and βGalCers with a β-hydroxylated acyl chain do not separate as much as corresponding GalCers with nonhydroxylated acyl chains, we also synthesized αGlcCers with a β-hydroxylated acyl chain. αGlcCer(d18:0/βh16:0) gives rise to a b/McL ratio of 1.78 ± 0.08 in MS^2, more related to αGalCer(d18:0/βh16:0) (b/McL = 2.93)

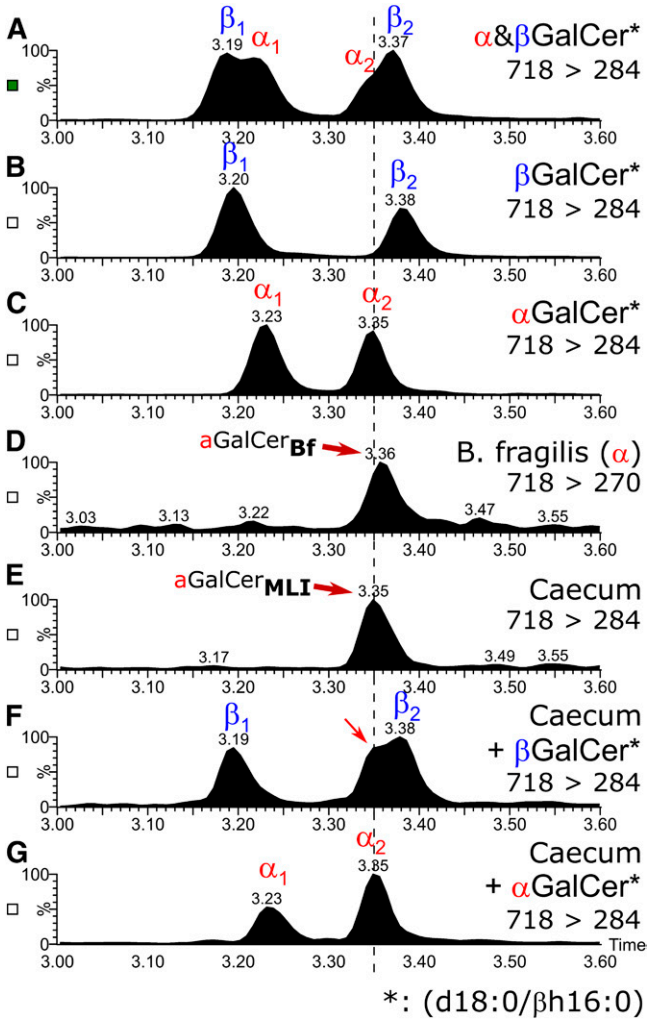

Fig. 4. HILIC-MS^2 of GalCer(d18:0/βh16:0) standards and αGalCer from *B. fragilis* in comparison with GalCer(d18:0/h16:0) from mouse cecum. Mixture of synthetic α- and βGalCer(d18:0;βh16:0) (A), synthetic βGalCer(d18:0/βh16:0) (B), synthetic αGalCer(d18:0/βh16:0) (C), αGalCer$_{Bf}$/αGalCer(d17:0/βh17:0) from *B. fragilis* (D), αGalCer$_{MLI}$ from mouse cecum (E), mixture of αGalCer$_{MLI}$ from mouse cecum with synthetic βGalCer(d18:0/βh16:0) (F), and mixture of αGalCer$_{MLI}$ from mouse cecum with synthetic αGalCer(d18:0/βh16:0) (G). Plotted are SRMs of the protonated compound to their respective dehydrated sphingoid base fragments. Note that αGalCer$_{MLI}$ from mouse cecum comigrates with the second peak of αGalCer(d18:0/βh16:0) (C), but not with βGalCer(d18:0/βh16:0) (B). Furthermore, a mixture of the cecum sample with βGalCer results in a broadened second peak with shoulder (F), but in a mixture of the cecum sample with αGalCer, the second peak remains sharp and increases in intensity with respect to the first peak (G). Note that samples of synthetic αGalCer or synthetic βGalCer contain a mixture of two diastereomers with respect to the *R*- or *S*-orientation of the β-hydroxy group of the fatty acid, the latter being used as a racemic compound for synthesis. As in RP18-LC (Fig. 3), this will lead to two separate peaks in HILIC, which are annotated as α_1/β_1 and α_2/β_2.

than to βGalCer(d18:0/βh16:0) (b/McL = 0.19). On the RP18-LC-MS^2 system, αGlcCer(d18:0/βh16:0) does not separate from the corresponding αGalCer(d18:0/βh16:0). However, on the HILIC-MS^2 system, both αGlcCer(d18:0/βh16:0) peaks, which are eluting almost identically, elute in front of the second αGalCer(d18:0/βh16:0). Because the latter corresponds to the compound found in the large intestine, this is an αGalCer and not an αGlcCer (supplemental Fig. S8).

High-resolution FT-ICR-MS^2 confirms the presence of HexCer(d18:0/βh16:0) in mouse cecum and the structural identity of CID-fragments

We subjected the αGalCer$_{MLI}$-enriched sample from mouse caeca to high-resolution FT-ICR-MS^2 and detected a peak at *m/z* 740.56468 differing by 0.167 ppm from the theoretical mass of the chemical formula of GalCer(d18:0;h16:0). CID of this peak revealed a product ion at *m/z* 528.35097 corresponding with a mass error of 0.534 ppm to the theoretical McL fragment and a product ion at *m/z* 486.34035 corresponding with an error of 0.473 ppm to fragment d, as annotated in the GalCer structure with a β-hydroxylated acyl chain (Fig. 2A), as well as a product ion at *m/z* 348.28759 corresponding to the McL ion with further loss of hexose ($C_6H_{12}O_6$) and an error of 0.833 ppm (supplemental Table S5). The latter is also observed in the product ion spectra of GalCer(d18:0/βh16:0) recorded by LC-ESI-(triple quadrupole)MS^2 (supplemental Fig. S2). The presence of the McL fragment confirmed the β-hydroxylated acyl chain and, again, the b/McL ratio of 3.58 resembled the ratio of 2.87 found in synthetic αGalCer and the ratio of 2.82 found in αGalCer$_{Bf}$, but clearly distinguished from the b/McL ratio of 0.13 found in synthetic βGalCer on the FT-ICR instrument.

Synthetic αGalCer$_{MLI}$ activates *i*NKT cells

Presented on CD1d by APCs, αGalCer binds the TCR of *i*NKT cells and induces the formation of an immunological synapse. This formation leads to *i*NKT cell activation and cytokine secretion. To investigate the effects of synthetic αGalCer, a DC/*i*NKT cell coculture system was used (34). When tested in vitro, all synthetic αGalCers were capable of inducing, in a dose-dependent fashion, IL-2 production by the *i*NKT cell hybridoma; the activation of which depending solely on the TCR (**Fig. 5A**). In contrast, all corresponding βGalCer structures failed to induce *i*NKT cell activation. The IL-2 production induced by the synthetic analog of αGalCer$_{MLI}$, i.e., αGalCer(d18:0/βh16:0), was comparable to that of αGalCer$_{Bf}$. The difference (lower IL-2 production) relative to the positive control, αGalCer(d18:0/t26:0) (KRN7000), which contains the very long chain cerotic acid (26:0) [αGalCer(t18:0;26:0)], is in line with a previous report (7). Similar to KRN7000, αGalCer(d18:1/24:1) with the very long chain nervonic acid (24:1) activated *i*NKT cells at lower concentrations than the other αGalCers, which comprised shorter C16-fatty acids. We then assessed the effect of αGalCer structures on primary *i*NKT cells. To this end, splenocytes from wild-type and *CD1d*$^{-/-}$ mice were exposed to purified glycolipids, and IFN-γ concentration was measured by ELISA. As depicted in Fig. 5B, synthetic αGalCers activated, in a CD1d-dependent manner, the release of IFN-γ by splenocytes. Collectively, synthetic αGalCer$_{MLI}$s activate *i*NKT cells in a CD1d-dependent manner.

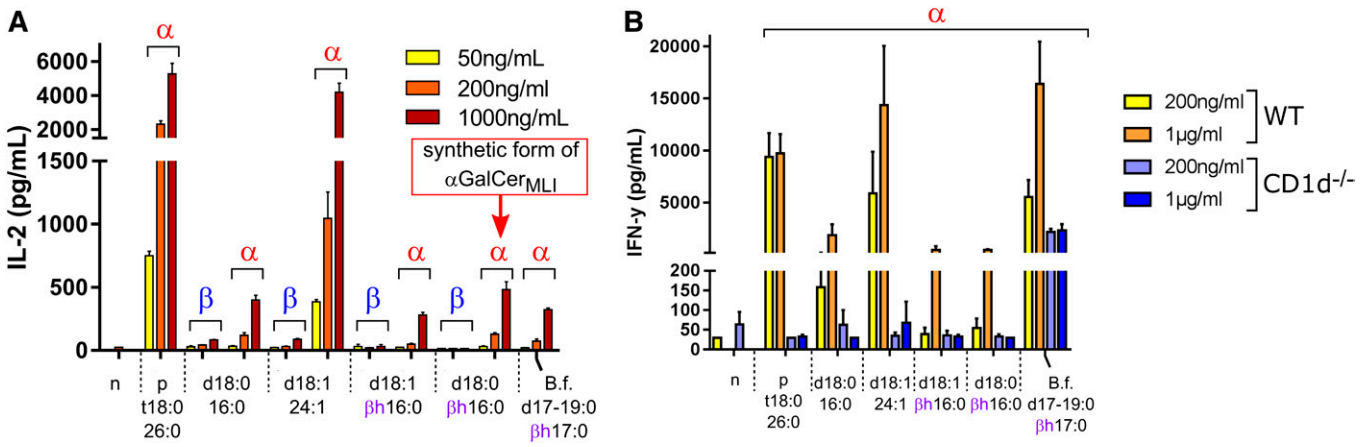

Fig. 5. Activation of *i*NKT cells by synthetic αGalCer and βGalCer. A: DCs and *i*NKT cells were cocultured in the presence of grading doses of synthetic β- or αGalCers (n = 3). B: Splenocytes from wild-type and *CD1d*$^{-/-}$ mice were exposed to synthetic αGalCers (n = 3). Coculture supernatants were collected at 24 h (IL-2) and 48 h (IFN-γ), respectively (triplicates ± SD). n, negative control (no lipid); p, positive control. Note that αGalCer with the ceramide anchor d18:0/βh16:0 corresponds in structure to αGalCer$_{MLI}$. *B.f.*, *B. fragilis* αGalCer(d(17/18/19):0/βh17:0). In contrast to the other synthetic compounds, αGalCer$_{Bf}$ was extracted from *B. fragilis* culture (8).

Stressful conditions alter the content of αGalCer$_{MLI}$ in the large intestine

Alterations of the intestinal microbiota composition are associated with a variety of diseases, including obesity, diabetes, and inflammatory bowel disease (35). Furthermore, diet is a major driving factor for the establishment of the gut microbiome, and a fat-rich diet is associated with the suppression of several bacteria, including a number of *Bacteroides* (36). Likewise, studies in mice revealed that obesity is associated with a division-wide increase in the relative abundance of the *Firmicutes* and a corresponding division-wide decrease in the relative abundance of the *Bacteroidetes* (37), which may produce αGalCer$_{MLI}$. To study the impact of diet on αGalCer$_{MLI}$ levels in the gut, C57BL/6 mice were fed for 7 days with WTD, which is rich in fat and sugar. After 7 days, total cecum was analyzed for the presence of αGalCer$_{MLI}$. Relative to the control, mice fed WTD had an almost 3-fold decrease of αGalCer$_{MLI}$ in the intestine (**Fig. 6A**).

We next turned to investigate the effect of a local inflammation (colitis) on the concentration of αGalCer$_{MLI}$. To this end, mice were treated with the heparin-like polysaccharide, DSS, a compound commonly used to induce inflammatory disorders of the colon such as inflammatory bowel diseases, principally, ulcerative colitis and Crohn's disease. This experimental model induces colitis in mice. Of note, *Bacteroidetes* were reported to significantly decrease in the colon after DSS treatment (38–41). Mice (C57BL/6) were treated with DSS for 4 days and samples were collected after 2 and 4 days. αGalCer$_{MLI}$ levels decreased progressively over time down to less than 3% on day 4 (Fig. 6B). Because the intestinal epithelial barrier can turn leaky during colitis, antigens and bacteria may get carried to the liver, which in mice is rich in *i*NKT cells. Therefore, we also analyzed liver for the presence of αGalCer$_{MLI}$ in the colitis model. Levels were below the detection limit in all samples (Fig. 6B, supplemental Fig. S9).

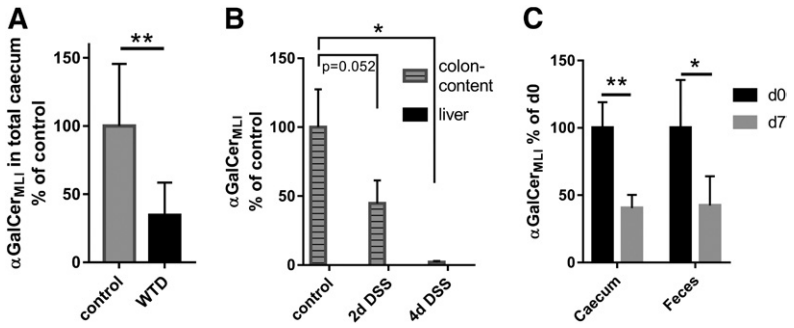

Fig. 6. Levels of intestinal and fecal αGalCer$_{MLI}$ are influenced by diet (A), inflammation (B), and viral infection (C). A: Male C57BL/6N mice (23–36 weeks old) were fed for 7 days with control or WTD and total cecum was analyzed for the presence of αGalCer(d18:0/βh16:0), i.e., αGalCer$_{MLI}$ (n = 8). B: Male C57BL/6 mice (9–11 weeks old) were treated with DSS to induce colitis. After 2 and 4 days, liver and the content of the colon were isolated and analyzed for αGalCer$_{MLI}$ (control and 2d DSS, n = 3; 4d DSS, n = 5). C: Male C57BL/6 mice (8 weeks old) were infected with influence virus A. Total cecum and feces were analyzed at day 0 (mock-treated noninfected mice) and at day 7 (cecum, n = 6; feces, n = 5). Data of A and B were obtained with RP18-LC-MS^2 and data of C with the HILIC-MS^2 method. For absolute values see supplemental Fig. S9.

Finally, we evaluated the influence of influenza infection on $\alpha GalCer_{MLI}$. Recently, gut dysbiosis has been reported upon experimental (H1N1 and H5N1) IAV infection with a peak at day 7 postinfection [(42–46) and unpublished observations, F. Trottein]. Interestingly, the levels of caecal and fecal $\alpha GalCer_{MLI}$ were reduced by more than 2-fold at day 7 post-influenza infection (Fig. 6C).

DISCUSSION

NKT cells are innate lymphocytes at the interface between innate and adaptive immunity, which impact initiation and regulation of immune responses (47). This may impact, for example, anti-tumor immunity in the liver, which appeared to be controlled by liver NKT cells via the gut microbiome (48, 49).

Via the cell surface receptor, CD1d, APCs present lipids to the TCR of invariant (or type I) NKT (*i*NKT) cells (47). Whereas a series of lipids that bind to CD1d have been published, only a few allow the formation of a stable CD1d-lipid-TCR trimeric complex, which leads to activation of *i*NKT cells, either in the thymus or in the periphery in the context of inflammation and infection. Lipids of endogenous or microbial origin are processed and loaded on CD1d inside APCs and are thereafter presented on the cell surface (47).

Pathogen-derived α-anomeric glycolipids include α-galacturonylceramide [αGalACer(t18:0;14:0)] from *Sphingomonas spp.*, 6′-acyl-α-glucosylcholesterol from *Helicobacter pylori*, α-galactosyldiacylglycerol [αGalDAG(18:1/16:0)] from *Borrelia burgdorferi*, and α-glucosyldiacylglycerol [αGlcDAG(18:1/16:0)] from *Streptococcus pneumoniae* (50–53). Most of these pathogen-derived lipids do not activate *i*NKT cells as strongly as the synthetic αGalCer agonist, KRN7000 (2), which contains a very long acyl chain and a phytosphingosine. It was based on the naturally strong agonist, Agelasphin 9b [αGalCer(t18:0/α(*R*)h24:0)] (6).

Endogenous self-lipids have been proposed to replace pathogenic lipids on CD1d to activate *i*NKT cells in case infecting bacteria fail to supply immunogenic lipid ligands. This process appears to depend on Hexb-subunit (54). Hexb is required for the formation of hexosaminidases (HexA and HexB) involved in glycosphingolipid degradation/processing in lysosomes. In this lysosomal compartment also CD1d loading takes place (55).

Recently host-derived α-glycosylceramides (56, 57) and simple gangliosides GM3 and GD3 (34) containing monounsaturated nervonic acid have been discussed to serve as endogenous lipid ligands. The latter were enriched after Toll-like receptor stimulation of APCs (34, 58). The former are αGalCers containing sphingosine and nonhydroxylated acyl chains, apparently produced by immune cells (56, 57). Similar αGalCer structures, but with sphinganine and saturated nonhydroxylated acyl chains, were also reported to be present in cow milk and likely occur in the thymus, supporting the potential of mammalian cells to produce endogenous αGalCers (25, 59). In our hands, αGalCer containing nervonic acid, especially, appeared to stimulate *i*NKT cells more efficiently than αGalCers with shorter (C16-C17) acyl chains (Fig. 5).

Interestingly, not only the positive selection of *i*NKT cells in the thymus, but also the neonatal maturation of *i*NKT cells in the gut epithelium is CD1d restricted (24, 50, 60). For the latter, gut microbiota-derived αGalCer or related compounds might be critical (24, 60). In this context, αGalCers synthesized by the commensal *B. fragilis* exert either an inhibitory effect preventing proliferation or a stimulatory effect favoring the development of *i*NKT cells. In studies with neonatal mice lacking access to bacterial sphingolipids, treatment with *B. fragilis* glycosphingolipids (GSL-Bf717/$\alpha GalCer_{Bf}$) reduced colonic *i*NKT cell numbers and conferred protection against oxazolone-induced colitis (9); however, these αGalCers from *B. fragilis* bind to CD1d and activate both mouse and human *i*NKT cells, in vitro and in vivo (7).

In the current study, we screened mouse intestinal tissue for αGalCers with our physico-chemical HILIC-MS^2 method. We did not detect significant amounts of αGalCer displaying the same structures as those of *B. fragilis*. However, we detected a signal for a very closely related structure and showed that it is indeed an αGalCer containing a β-hydroxylated acyl chain [$\alpha GalCer_{MLI}$, i.e., αGalCer(d18:0;βh16:0)]. This $\alpha GalCer_{MLI}$ was, on the contrary, basically absent in corresponding lipid extracts from *B. fragilis* (supplemental Fig. S6I–L). Identification was achieved in comparison to corresponding synthetic α- and β-anomeric GalCers and related compounds. Although characteristically different retention times for α- and β-anomeric compounds diminished in GalCers containing a β-hydroxylated acyl chain compared to those with a nonhydroxylated acyl chain, the intensity ratios of specific fragments obtained from the sodiated molecular ions could be used to clearly annotate the anomeric linkage of the glycosidic bond. In contrast to GalCers with nonhydroxylated acyl chains, we did not use the ratio of fragments b and c (see Fig. 2), which had been reported lately (25), but the ratio of fragment b to the fragment specific for the presence of β-hydroxylated fatty acids, the McL fragment. Interestingly, this fragment is nicely observed from the sodiated but not the protonated molecular ions. As the McL fragment appears much more intense than fragment c, the sensitivity to screen biological samples for the presence of αGalCers with a β-hydroxylated acyl chain increases manifold using corresponding MRM transitions, while adding structural information. Both features, α-glycosidic linkage and β-hydroxylation of the acyl chain, are given by the αGalCer structures found in *B. fragilis*. Interestingly, αGalCer(d17:0;βh17:0) from *B. fragilis* ($\alpha GalCer_{Bf}$) migrated with HILIC identically to $\alpha GalCer_{MLI}$ as well as the second of the double peaks of synthetic αGalCer(d18:0;βh16:0) (Fig. 4). This $\alpha GalCer_{Bf}$ has previously been shown to contain a β*R*-hydroxylated acyl chain (7). Because the hydrophobic part of the ceramide anchor rather does not interact with the stationary phase in HILIC, it is therefore likely that the second peak of the synthetic standard corresponds to the β*R*-hydroxylated isomer. This implies that $\alpha GalCer_{MLI}$, like $\alpha GalCer_{Bf}$, contains a β*R*-hydroxylated

acyl chain. Differences arise in the length of the sphingoid base and *N*-linked acyl chain, but the total amount of C-atoms in the ceramide anchor of $\alpha GalCer_{MLI}$ was identical to the main αGalCer (GSL-Bf717) of *B. fragilis*. Therefore, it is not surprising that the synthetic $\alpha GalCer_{MLI}$ activated *i*NKT cells in a coculture system with similar results as $\alpha GalCer_{Bf}$. $\alpha GalCer_{MLI}$ was present in cecum (an extremely rich source of commensals) but not in duodenum and jejunum, arguing for a microbial- instead of a host-derived origin. Moreover, germ-free mice did not reveal this compound in their intestinal tract samples, here too arguing for a microbial origin of the $\alpha GalCer_{MLI}$. The structure of the *i*NKT-stimulatory $\alpha GalCer_{MLI}$ described in the current study might well be the enterogenous bacterial αGalCer-like glycolipid reported by Wei et al. (23). In the later study, the authors used the monoclonal antibody, L363, described to recognize a CD1d-complex with αGalCer or with a structurally related lipid.

As we found the identical structure in C57BL/6 and NMRI mice (Fig. 1) and in mice from four different facilities [three academic (Fig. 6) and one commercial (supplemental Fig. S10)], we exclude a strain-specific or facility-specific event. Nevertheless, absolute concentrations may depend on strain (supplemental Fig. S10). Because germ-free mice, lacking $\alpha GalCer_{MLI}$, obtained the same food as control mice, we exclude food as a source of this compound. Therefore, we conclude that the common microbiota of the mouse gut produce the $\alpha GalCer_{MLI}$ identified here. Considering that microbial αGalCer components were found in *Bacteroides* and *Prevotella* species of the human gut microbiome (7, 8), we hypothesized that the identified $\alpha GalCer_{MLI}$ may be part of the *Bacteriodetes* taxa. Previous publications showed the correlation between specific diets and the composition of the microbiome, especially the change in the ratio of *Firmicutes* versus *Bacteroidetes* [see reviews (61, 62)]. As this $\alpha GalCer_{MLI}$ corresponds in functional activity to $\alpha GalCer_{Bf}$, it may be speculated that, together with corresponding symbionts, it contributes to the microbiome-dependent neonatal maturation of *i*NKT cells in the gut epithelium, as has been reported lately (24, 50, 60). Both, $\alpha GalCer_{Bf}$ and $\alpha GalCer_{MLI}$ are not such strong inducers of *i*NKT cell activation as is the synthetic agonist, KRN7000, with its very long acyl chain, as demonstrated for $\alpha GalCer_{Bf}$ in supplemental Fig. 3 of Ref. 7. This may be attributed to the fact that the microbial compounds integrate a shorter acyl chain (C16 but not C26) and do not present a 4-hydroxy group in their sphingoid base (63–65). The incorporation of a shorter (C16-C17) acyl chain into αGalCers of commensals (going along with lower *i*NKT activation) might have developed evolutionarily to prevent inflammation against commensals. The β-hydroxylation of the *N*-linked acyl chain, however, appears to have little influence, if at all. The IL-2 and IFN-γ responses were similar upon stimulation with nonhydroxylated or β-hydroxylated acyl chains containing αGalCer (Fig. 5). To date, there is no established enzymatic pathway integrating β-hydroxylated acyl chains into mammalian sphingolipids, and it may turn out that β-hydroxylation could preferentially hint to a microbial origin of corresponding sphingolipids, although a ceramide with a β-hydroxylated acyl chain, i.e., Cer(d18;1;βh26:0), had been described for mouse epidermis (66, 67), another organ colonized with commensals. In contrast to the odd and iso-branched sphingoid base found in $\alpha GalCer_{Bf}$, the even and presumably unbranched sphingoid base of $\alpha GalCer_{MLI}$ is also found in mammalian tissue, which therefore cannot be excluded as a corresponding source for the base. Likewise, uptake and potential processing of $\alpha GalCer_{MLI}$ in mammalian lysosomes eventually could lead to de- and reacylation, e.g., by acidic ceramidase, leading to "mammalian-like" αGalCer. To reveal such processes, lysosomal degradation of exogenous αGalCer should be investigated in more detail.

Assuming that the $\alpha GalCer_{MLI}$ was of microbial origin, we thought its intestinal levels should depend on the composition of the microbiota and should reflect changes in the microbiome composition described in the literature.

Because diet is a major driving factor for the establishment of the gut microbiome, we evaluated the influence of WTD and observed an almost 3-fold decrease of $\alpha GalCer_{MLI}$ with this diet after only 1 week. Other studies in mice have previously revealed that obesity is associated with an increased relative abundance of *Firmicutes* and a decreased relative abundance of *Bacteroidetes* (37, 68). Bacteria described to produce αGalCer with β-hydroxylated acyl chains indeed belong to the latter phylum (7, 8). Low levels of *Bacteroides* were also reported in obesity/metabolic disorder (36, 69) in line with a relative depletion of *Bacteroides* in neonates exposed to maternal high-fat gestational diet (70).

Bacteroidetes were also reported to decrease in a commonly used model of experimental colitis induced by DSS (41). Decreased *Bacteroides* levels are associated with inflammatory bowel disease and ulcerative colitis (36, 71) and a decreased abundance of *Erysipelotrichales*, *Bacteroidales*, and *Clostridiales* going along with an increase of *Enterobacteriaceae*, *Pasteurellacaea*, Veillonellaceae, and *Fusobacteriaceae* were observed in new-onset cases of pediatric Crohn's disease (72). The loss of *Bacteroidetes* would correlate the strong decrease of $\alpha GalCer_{MLI}$, which we observed in a model of DSS-induced colitis. The over 30-fold decrease indicates special sensitivity of αGalCer-producing bacteria to inflammatory disorders of the colon.

Infections primarily not targeting the intestinal tract nevertheless impact the gut microbiome. IAV infection, for example, leads to enteric dysbiosis in the mouse system, and possibly in humans [(42–46) and unpublished observations, F. Trottein]. Our data show that mice infected 7 days earlier with IAV (the peak of lung inflammation) displayed a reduced amount of $\alpha GalCer_{MLI}$ relative to non-infected animals. Several changes in the gut microbiome have been observed after infection with IAV. Especially, the *Bacteroidetes* S24-7 family to which the potential αGalCer-producing *Bacteroides* belong decreased on day 7 postinfection [(42) and unpublished observations, F. Trottein].

Collectively, our data reveal for the first time the presence of an αGalCer [$\alpha GalCer_{MLI}$, which is αGalCer(d18:0;βh16:0)] in the digestive tract of mice, which is very likely of microbial

origin, and demonstrate that stressful conditions altering the microbiome composition impact strongly on its production. These findings raise interesting questions concerning the potential impact of such αGalCer alteration on functions and activation status of *i*NKT cells and a corresponding impact on global immunity.

Note added in proof

There was an error in Supplemental Table 3 in the version of this article that was published as a Paper in Press on September 4, 2019. In column 2, the precursor ion labels $[M+H]^+$ and $[M+H\text{-}H_2O]^+$ were inadvertently switched. This error has now been corrected in the online version.

The authors thank Benita von Tümpling-Radosta for excellent technical assistance. Albert Bendelac (University of Chicago) is acknowledged for providing DN32 cells and Luc Van Kaer (Vanderbilt University, Nashville, TN) for the gift of the *CD1d*$^{-/-}$ mice. Christophe Paget (University of Tours) is acknowledged for the critical reading of this manuscript. R.S. thanks the German Research Foundation ("Deutsche Forschungsgemeinschaft") for funding within the Transregional Collaborative Research Centre 156. C.H. thanks the Deutsche Forschungsgemeinschaft for the funding of a SolariX FTICR MS (INST 874/7-1 FUGG).

REFERENCES

1. D'Souza, M. P., E. Adams, J. D. Altman, M. E. Birnbaum, C. Boggiano, G. Casorati, Y. H. Chien, A. Conley, S. B. G. Eckle, K. Fruh, et al. 2019. Casting a wider net: immunosurveillance by nonclassical MHC molecules. *PLoS Pathog.* **15:** e1007567.
2. Morita, M., K. Motoki, K. Akimoto, T. Natori, T. Sakai, E. Sawa, K. Yamaji, Y. Koezuka, E. Kobayashi, and H. Fukushima. 1995. Structure-activity relationship of alpha-galactosylceramides against B16-bearing mice. *J. Med. Chem.* **38:** 2176–2187.
3. Kawano, T., J. Cui, Y. Koezuka, I. Toura, Y. Kaneko, K. Motoki, H. Ueno, R. Nakagawa, H. Sato, E. Kondo, et al. 1997. CD1d-restricted and TCR-mediated activation of valpha14 NKT cells by glycosylceramides. *Science.* **278:** 1626–1629.
4. Kronenberg, M. 2005. Toward an understanding of NKT cell biology: progress and paradoxes. *Annu. Rev. Immunol.* **23:** 877–900.
5. Vartabedian, V. F., P. B. Savage, and L. Teyton. 2016. The processing and presentation of lipids and glycolipids to the immune system. *Immunol. Rev.* **272:** 109–119.
6. Natori, T., Y. Koezuka, and T. Higa. 1993. Agelasphins, novel alpha-galactosylceramides from the marine sponge Agelas mauritianus. *Tetrahedron Lett.* **34:** 5591–5592.
7. Wieland Brown, L. C., C. Penaranda, P. C. Kashyap, B. B. Williams, J. Clardy, M. Kronenberg, J. L. Sonnenburg, L. E. Comstock, J. A. Bluestone, and M. A. Fischbach. 2013. Production of alpha-galactosylceramide by a prominent member of the human gut microbiota. *PLoS Biol.* **11:** e1001610.
8. von Gerichten, J., K. Schlosser, D. Lamprecht, I. Morace, M. Eckhardt, D. Wachten, R. Jennemann, H. J. Grone, M. Mack, and R. Sandhoff. 2017. Diastereomer-specific quantification of bioactive hexosylceramides from bacteria and mammals. *J. Lipid Res.* **58:** 1247–1258.
9. An, D., S. F. Oh, T. Olszak, J. F. Neves, F. Y. Avci, D. Erturk-Hasdemir, X. Lu, S. Zeissig, R. S. Blumberg, and D. L. Kasper. 2014. Sphingolipids from a symbiotic microbe regulate homeostasis of host intestinal natural killer T cells. *Cell.* **156:** 123–133.
10. Rabionet, M., K. Gorgas, and R. Sandhoff. 2014. Ceramide synthesis in the epidermis. *Biochim. Biophys. Acta.* **1841:** 422–434.
11. Kihara, A. 2016. Synthesis and degradation pathways, functions, and pathology of ceramides and epidermal acylceramides. *Prog. Lipid Res.* **63:** 50–69.
12. Nojima, H., C. M. Freeman, E. Gulbins, and A. B. Lentsch. 2015. Sphingolipids in liver injury, repair and regeneration. *Biol. Chem.* **396:** 633–643.
13. Saddoughi, S. A., P. Song, and B. Ogretmen. 2008. Roles of bioactive sphingolipids in cancer biology and therapeutics. *Subcell. Biochem.* **49:** 413–440.
14. Hannun, Y. A., and L. M. Obeid. 2008. Principles of bioactive lipid signalling: lessons from sphingolipids. *Nat. Rev. Mol. Cell Biol.* **9:** 139–150.
15. Itokazu, Y., J. Wang, and R. K. Yu. 2018. Gangliosides in nerve cell specification. *Prog. Mol. Biol. Transl. Sci.* **156:** 241–263.
16. Grösch, S., A. V. Alessenko, and E. Albi. 2018. The many facets of sphingolipids in the specific phases of acute inflammatory response. *Mediators Inflamm.* **2018:** 5378284.
17. Sohlenkamp, C., and O. Geiger. 2016. Bacterial membrane lipids: diversity in structures and pathways. *FEMS Microbiol. Rev.* **40:** 133–159.
18. Geiger, O., N. Gonzalez-Silva, I. M. Lopez-Lara, and C. Sohlenkamp. 2010. Amino acid-containing membrane lipids in bacteria. *Prog. Lipid Res.* **49:** 46–60.
19. Kato, M., Y. Muto, K. Tanaka-Bandoh, K. Watanabe, and K. Ueno. 1995. Sphingolipid composition in Bacteroides species. *Anaerobe.* **1:** 135–139.
20. Wick, E. C., and C. L. Sears. 2010. Bacteroides spp. and diarrhea. *Curr. Opin. Infect. Dis.* **23:** 470–474.
21. Rhee, K. J., S. Wu, X. Wu, D. L. Huso, B. Karim, A. A. Franco, S. Rabizadeh, J. E. Golub, L. E. Mathews, J. Shin, et al. 2009. Induction of persistent colitis by a human commensal, enterotoxigenic Bacteroides fragilis, in wild-type C57BL/6 mice. *Infect. Immun.* **77:** 1708–1718.
22. An, D., C. Na, J. Bielawski, Y. A. Hannun, and D. L. Kasper. 2011. Membrane sphingolipids as essential molecular signals for Bacteroides survival in the intestine. *Proc. Natl. Acad. Sci. USA.* **108 (Suppl. 1):** 4666–4671.
23. Wei, Y., B. Zeng, J. Chen, G. Cui, C. Lu, W. Wu, J. Yang, H. Wei, R. Xue, L. Bai, et al. 2016. Enterogenous bacterial glycolipids are required for the generation of natural killer T cells mediated liver injury. *Sci. Rep.* **6:** 36365.
24. Wingender, G., D. Stepniak, P. Krebs, L. Lin, S. McBride, B. Wei, J. Braun, S. K. Mazmanian, and M. Kronenberg. 2012. Intestinal microbes affect phenotypes and functions of invariant natural killer T cells in mice. *Gastroenterology.* **143:** 418–428.
25. Brennan, P. J., T. Y. Cheng, D. G. Pellicci, G. F. M. Watts, N. Veerapen, D. C. Young, J. Rossjohn, G. S. Besra, D. I. Godfrey, M. B. Brenner, et al. 2017. Structural determination of lipid antigens captured at the CD1d-T-cell receptor interface. *Proc. Natl. Acad. Sci. USA.* **114:** 8348–8353.
26. Vetere, A., M. W. Alachraf, S. K. Panda, J. T. Andersson, and W. Schrader. 2018. Studying the fragmentation mechanism of selected components present in crude oil by collision-induced dissociation mass spectrometry. *Rapid Commun. Mass Spectrom.* **32:** 2141–2151.
27. Abbes, I., C. Rihouey, J. Hardouin, T. Jouenne, E. De, and S. Alexandre. 2018. Identification by mass spectrometry of glucosaminylphosphatidylglycerol, a phosphatidylglycerol derivative, produced by Pseudomonas aeruginosa. *Rapid Commun. Mass Spectrom.* **32:** 2113–2121.
28. Rovillos, M. J., J. K. Pauling, H. K. Hannibal-Bach, C. Vionnet, A. Conzelmann, and C. S. Ejsing. 2016. Structural characterization of suppressor lipids by high-resolution mass spectrometry. *Rapid Commun. Mass Spectrom.* **30:** 2215–2227.
29. Jennemann, R., R. Sandhoff, L. Langbein, S. Kaden, U. Rothermel, H. Gallala, K. Sandhoff, H. Wiegandt, and H. J. Grone. 2007. Integrity and barrier function of the epidermis critically depend on glucosylceramide synthesis. *J. Biol. Chem.* **282:** 3083–3094.
30. Sandhoff, R., S. T. Hepbildikler, R. Jennemann, R. Geyer, V. Gieselmann, R. L. Proia, H. Wiegandt, and H. J. Grone. 2002. Kidney sulfatides in mouse models of inherited glycosphingolipid disorders: determination by nano-electrospray ionization tandem mass spectrometry. *J. Biol. Chem.* **277:** 20386–20398.
31. Eley, A., D. Greenwood, and F. O'Grady. 1985. Comparative growth of Bacteroides species in various anaerobic culture media. *J. Med. Microbiol.* **19:** 195–201.
32. Beshara, R., V. Sencio, D. Soulard, A. Barthelemy, J. Fontaine, T. Pinteau, L. Deruyter, M. B. Ismail, C. Paget, J. C. Sirard, et al. 2018. Alteration of Flt3-Ligand-dependent de novo generation of conventional dendritic cells during influenza infection contributes to respiratory bacterial superinfection. *PLoS Pathog.* **14:** e1007360.
33. Hsu, F. F. 2016. Complete structural characterization of ceramides as [M-H](-) ions by multiple-stage linear ion trap mass spectrometry. *Biochimie.* **130:** 63–75.

34. Paget, C., S. Deng, D. Soulard, D. A. Priestman, S. Speca, J. von Gerichten, A. O. Speak, A. Saroha, Y. Pewzner-Jung, A. H. Futerman, et al. 2019. TLR9-mediated dendritic cell activation uncovers mammalian ganglioside species with specific ceramide backbones that activate invariant natural killer T cells. *PLoS Biol.* **17:** e3000169.
35. Harusato, A., and B. Chassaing. 2018. Insights on the impact of diet-mediated microbiota alterations on immunity and diseases. *Am. J. Transplant.* **18:** 550–555.
36. Lee, Y. K. 2013. Effects of diet on gut microbiota profile and the implications for health and disease. *Biosci. Microbiota Food Health.* **32:** 1–12.
37. Ley, R. E., F. Backhed, P. Turnbaugh, C. A. Lozupone, R. D. Knight, and J. I. Gordon. 2005. Obesity alters gut microbial ecology. *Proc. Natl. Acad. Sci. USA.* **102:** 11070–11075.
38. Tóth, G., R. F. Murphy, and S. Lovas. 2001. Stabilization of local structures by pi-CH and aromatic-backbone amide interactions involving prolyl and aromatic residues. *Protein Eng.* **14:** 543–547.
39. Pinho, R. A., P. C. Silveira, L. A. Silva, E. Luiz Streck, F. Dal-Pizzol, and J. C. F. Moreira. 2005. N-acetylcysteine and deferoxamine reduce pulmonary oxidative stress and inflammation in rats after coal dust exposure. *Environ. Res.* **99:** 355–360.
40. Laroui, H., S. A. Ingersoll, H. C. Liu, M. T. Baker, S. Ayyadurai, M. A. Charania, F. Laroui, Y. Yan, S. V. Sitaraman, and D. Merlin. 2012. Dextran sodium sulfate (DSS) induces colitis in mice by forming nano-lipocomplexes with medium-chain-length fatty acids in the colon. *PLoS One.* **7:** e32084.
41. Zhang, P., H. Jiao, C. Wang, Y. Lin, and S. You. 2019. Chlorogenic acid ameliorates colitis and alters colonic microbiota in a mouse model of dextran sulfate sodium-induced colitis. *Front. Physiol.* **10:** 325.
42. Yildiz, S., B. Mazel-Sanchez, M. Kandasamy, B. Manicassamy, and M. Schmolke. 2018. Influenza A virus infection impacts systemic microbiota dynamics and causes quantitative enteric dysbiosis. *Microbiome.* **6:** 9.
43. Bartley, J. M., X. Zhou, G. A. Kuchel, G. M. Weinstock, and L. Haynes. 2017. Impact of age, caloric restriction, and influenza infection on mouse gut microbiome: an exploratory study of the role of age-related microbiome changes on influenza responses. *Front. Immunol.* **8:** 1164.
44. Deriu, E., G. M. Boxx, X. He, C. Pan, S. D. Benavidez, L. Cen, N. Rozengurt, W. Shi, and G. Cheng. 2016. Influenza virus affects intestinal microbiota and secondary salmonella infection in the gut through type I interferons. *PLoS Pathog.* **12:** e1005572.
45. Qin, N., B. Zheng, J. Yao, L. Guo, J. Zuo, L. Wu, J. Zhou, L. Liu, J. Guo, S. Ni, et al. 2015. Influence of H7N9 virus infection and associated treatment on human gut microbiota. *Sci. Rep.* **5:** 14771.
46. Wang, J., F. Li, H. Wei, Z. X. Lian, R. Sun, and Z. Tian. 2014. Respiratory influenza virus infection induces intestinal immune injury via microbiota-mediated Th17 cell-dependent inflammation. *J. Exp. Med.* **211:** 2397–2410.
47. Bendelac, A., P. B. Savage, and L. Teyton. 2007. The biology of NKT cells. *Annu. Rev. Immunol.* **25:** 297–336.
48. Ma, C., M. Han, B. Heinrich, Q. Fu, Q. Zhang, M. Sandhu, D. Agdashian, M. Terabe, J. A. Berzofsky, V. Fako, et al. 2018. Gut microbiome-mediated bile acid metabolism regulates liver cancer via NKT cells. *Science.* **360:** eaan5931.
49. Schramm, C. 2018. Bile acids, the microbiome, immunity, and liver tumors. *N. Engl. J. Med.* **379:** 888–890.
50. Kumar, A., N. Suryadevara, T. M. Hill, J. S. Bezbradica, L. Van Kaer, and S. Joyce. 2017. Natural killer T cells: an ecological evolutionary developmental biology perspective. *Front. Immunol.* **8:** 1858.
51. Wu, D., G. W. Xing, M. A. Poles, A. Horowitz, Y. Kinjo, B. Sullivan, V. Bodmer-Narkevitch, O. Plettenburg, M. Kronenberg, M. Tsuji, et al. 2005. Bacterial glycolipids and analogs as antigens for CD1d-restricted NKT cells. *Proc. Natl. Acad. Sci. USA.* **102:** 1351–1356.
52. Sriram, V., W. Du, J. Gervay-Hague, and R. R. Brutkiewicz. 2005. Cell wall glycosphingolipids of Sphingomonas paucimobilis are CD1d-specific ligands for NKT cells. *Eur. J. Immunol.* **35:** 1692–1701.
53. Kinjo, Y., D. Wu, G. Kim, G. W. Xing, M. A. Poles, D. D. Ho, M. Tsuji, K. Kawahara, C. H. Wong, and M. Kronenberg. 2005. Recognition of bacterial glycosphingolipids by natural killer T cells. *Nature.* **434:** 520–525.
54. Mattner, J., K. L. Debord, N. Ismail, R. D. Goff, C. Cantu 3rd, D. Zhou, P. Saint-Mezard, V. Wang, Y. Gao, N. Yin, et al. 2005. Exogenous and endogenous glycolipid antigens activate NKT cells during microbial infections. *Nature.* **434:** 525–529.
55. Sandhoff, R., and K. Sandhoff. 2018. Emerging concepts of ganglioside metabolism. *FEBS Lett.* **592:** 3835–3864.
56. Kain, L., B. Webb, B. L. Anderson, S. Deng, M. Holt, A. Costanzo, M. Zhao, K. Self, A. Teyton, C. Everett, et al. 2014. The identification of the endogenous ligands of natural killer T cells reveals the presence of mammalian alpha-linked glycosylceramides. *Immunity.* **41:** 543–554. [Erratum. 2014. *Immunity.* 41: 867.]
57. Kain, L., A. Costanzo, B. Webb, M. Holt, A. Bendelac, P. B. Savage, and L. Teyton. 2015. Endogenous ligands of natural killer T cells are alpha-linked glycosylceramides. *Mol. Immunol.* **68:** 94–97.
58. Paget, C., T. Mallevaey, A. O. Speak, D. Torres, J. Fontaine, K. C. Sheehan, M. Capron, B. Ryffel, C. Faveeuw, M. Leite de Moraes, et al. 2007. Activation of invariant NKT cells by toll-like receptor 9-stimulated dendritic cells requires type I interferon and charged glycosphingolipids. *Immunity.* **27:** 597–609.
59. Brennan, P. J., R. V. Tatituri, C. Heiss, G. F. Watts, F. F. Hsu, N. Veerapen, L. R. Cox, P. Azadi, G. S. Besra, and M. B. Brenner. 2014. Activation of iNKT cells by a distinct constituent of the endogenous glucosylceramide fraction. *Proc. Natl. Acad. Sci. USA.* **111:** 13433–13438.
60. Olszak, T., D. An, S. Zeissig, M. P. Vera, J. Richter, A. Franke, J. N. Glickman, R. Siebert, R. M. Baron, D. L. Kasper, et al. 2012. Microbial exposure during early life has persistent effects on natural killer T cell function. *Science.* **336:** 489–493.
61. Louis, P., G. L. Hold, and H. J. Flint. 2014. The gut microbiota, bacterial metabolites and colorectal cancer. *Nat. Rev. Microbiol.* **12:** 661–672.
62. Santos-Marcos, J. A., C. Haro, A. Vega-Rojas, J. F. Alcala-Diaz, H. Molina-Abril, A. Leon-Acuna, J. Lopez-Moreno, B. B. Landa, M. Tena-Sempere, P. Perez-Martinez, et al. 2019. Sex differences in the gut microbiota as potential determinants of gender predisposition to disease. *Mol. Nutr. Food Res.* **63:** e1800870.
63. McCarthy, C., D. Shepherd, S. Fleire, V. S. Stronge, M. Koch, P. A. Illarionov, G. Bossi, M. Salio, G. Denkberg, F. Reddington, et al. 2007. The length of lipids bound to human CD1d molecules modulates the affinity of NKT cell TCR and the threshold of NKT cell activation. *J. Exp. Med.* **204:** 1131–1144.
64. Goff, R. D., Y. Gao, J. Mattner, D. P. Zhou, N. Yin, C. Cantu, L. Teyton, A. Bendelac, and P. B. Savage. 2004. Effects of lipid chain lengths in alpha-galactosylceramides on cytokine release by natural killer T cells. *J. Am. Chem. Soc.* **126:** 13602–13603.
65. Veerapen, N., S. S. Kharkwal, P. Jervis, V. Bhowruth, A. K. Besra, S. J. North, S. M. Haslam, A. Dell, J. Hobrath, P. J. Quaid, et al. 2018. Photoactivable glycolipid antigens generate stable conjugates with CD1d for invariant natural killer T cell activation. *Bioconjug. Chem.* **29:** 3161–3173.
66. Madison, K. C., D. C. Swartzendruber, P. W. Wertz, and D. T. Downing. 1990. Sphingolipid metabolism in organotypic mouse keratinocyte cultures. *J. Invest. Dermatol.* **95:** 657–664.
67. Tsugawa, H., K. Ikeda, W. Tanaka, Y. Senoo, M. Arita, and M. Arita. 2017. Comprehensive identification of sphingolipid species by in silico retention time and tandem mass spectral library. *J. Cheminform.* **9:** 19.
68. Turnbaugh, P. J., F. Backhed, L. Fulton, and J. I. Gordon. 2008. Diet-induced obesity is linked to marked but reversible alterations in the mouse distal gut microbiome. *Cell Host Microbe.* **3:** 213–223.
69. Fava, F., R. Gitau, B. A. Griffin, G. R. Gibson, K. M. Tuohy, and J. A. Lovegrove. 2013. The type and quantity of dietary fat and carbohydrate alter faecal microbiome and short-chain fatty acid excretion in a metabolic syndrome 'at-risk' population. *Int. J. Obes. (Lond.).* **37:** 216–223.
70. Chu, D. M., K. M. Antony, J. Ma, A. L. Prince, L. Showalter, M. Moller, and K. M. Aagaard. 2016. The early infant gut microbiome varies in association with a maternal high-fat diet. *Genome Med.* **8:** 77.
71. Sun, M., B. Du, Y. Shi, Y. Lu, Y. Zhou, and B. Liu. 2019. Combined signature of the fecal microbiome and plasma metabolome in patients with ulcerative colitis. *Med. Sci. Monit.* **25:** 3303–3315.
72. Gevers, D., S. Kugathasan, L. A. Denson, Y. Vazquez-Baeza, W. Van Treuren, B. Ren, E. Schwager, D. Knights, S. J. Song, M. Yassour, et al. 2014. The treatment-naive microbiome in new-onset Crohn's disease. *Cell Host Microbe.* **15:** 382–392.